ChemPhysChem

Research Article
doi.org/10.1002/cphc.202400274

Chemistry Europe
European Chemical Societies Publishing

www.chemphyschem.org

Solving the Puzzle of the Carbonic Acid Vibrational Spectrum – an Anharmonic Story

Jonas Schlagin,[a] Dennis F. Dinu,[a] Jürgen Bernard,[b] Thomas Loerting,[b] Hinrich Grothe,[c] and Klaus R. Liedl*[a]

Against the general belief that carbonic acid is too unstable for synthesis, it was possible to synthesize the solid[1,2] as well as gas-phase carbonic acid.[3] It was suggested that solid carbonic acid might exist in Earth's upper troposphere and in the harsh environments of other solar bodies,[4] where it undergoes a cycle of synthesis, decomposition, and dimerization.[5] To provide spectroscopic data for probing the existence of extraterrestrial carbonic acid,[2,6] matrix-isolation infrared (MI–IR) spectroscopy has shown to be essential.[3,4,6–8] However, early assignments within the harmonic approximation using scaling factors impeded a full interpretation of the rather complex MI–IR spectrum of H_2CO_3. Recently, carbonic acid was detected in the Galactic center molecular cloud,[9] triggering new interest in the anharmonic spectrum.[10] In this regard, we substantially reassign our argon MI–IR spectra based on accurate anharmonic calculations. We calculate a four-mode potential energy surface (PES) at the explicitly correlated coupled-cluster theory using up to triple-zeta basis sets, i.e., CCSD(T)-F12/cc-pVTZ–F12. On this PES, we perform vibrational self-consistent field and configuration interaction (VSCF/VCI) calculations to obtain accurate vibrational transition frequencies and resonance analysis of the fundamentals, first overtones, and combination bands. In total, 12 new bands can be assigned, extending the spectral data for carbonic acid and thus simplifying detection in more complex environments. Furthermore, we clarify disputed assignments between the cc- and ct-conformer.

Introduction

The recent observation of carbonic acid (CA, H_2CO_3) in the Galactic center molecular cloud G + 0.693–0.027 through millimeter wave radio spectroscopy[9] has triggered new efforts in experimental and computational spectroscopy of CA.[10] CA is considered a promising candidate to be observed in the JWST data.[10] However, providing laboratory reference data for CA is not straightforward. It is well-known that CA is short-lived[11] and rapidly decomposes into H_2O and CO_2 in aqueous environments (e.g. carbonate buffer):[12,13]

$$H_2O + CO_2 \rightleftharpoons H_2CO_3 \overset{H^+}{\rightleftharpoons} HCO_3^- \overset{H^+}{\rightleftharpoons} CO_3^{2-}$$

CA evaded early attempts of laboratory observation in the 1960s[14] and was considered too labile to be isolated.[15,16] This sparked a series of quantum mechanical studies regarding thermodynamic stability,[15–21] the reaction pathway of decomposition,[22,23] and the force constants.[24] These calculations suggested three distinct minima structures (cf. Figure 1), with the cc-conformer being the most stable, followed by the ct- and tt-conformer.[25]

In 1973, Behrendt et al. succeeded in the synthesis of monoetherated CA adducts and their salts.[26,27] In 1987, Schwarz et al. identified the m/z signal of CA radical cations obtained via thermolysis of NH_4HCO_3, providing the first evidence of stable CA in the gas phase.[28] In 1990, Falcke et al. accumulated CA by exploiting the slower dehydration of CA compared to the protonation of the carbonates (HCO_3^-,CO_3^{2-}), and identified the first spectral features of CA via Raman spectroscopy.[29]

Ever since, several solid-state syntheses of CA and deuterated CA were established, including the proton irradiation of 1:1 H_2O:CO_2 ice-mixtures,[30] acid-base reactions of glassy solutions,[1,2] the bombardment of CO_2 with H^+/He,[31] the electronic discharge of CO_2:Ar gas mixtures in water[32] and the pyrolysis of higher organocarbonates.[8]

Follow-up studies of solid CA identified a tight temperature range in which CA can be sublimated and resublimated without decomposition.[5] This also allowed the study of the spectral features of gaseous CA. The CA synthesis conditions led to the assumption that CA could be observable in certain extraterrestrial and other extreme environments. Besides comets, the Martian surface and the surface of other solar bodies,[5,33] where it undergoes a cycle of formation, decomposition, and dimerization, the Earth's upper troposphere in cirrus clouds and mineral dust particles have been suggested.[4,34] The latter was shown at

[a] J. Schlagin, Dr. D. F. Dinu, Univ.-Prof. Dr. K. R. Liedl
Institute of General, Inorganic and Theoretical Chemistry
University of Innsbruck
Innrain 80–82, 6020 Innsbruck
E-mail: Klaus.Liedl@uibk.ac.at

[b] Dr. J. Bernard, Assoc. Prof. Dr. T. Loerting
Institute of Physical Chemistry
University of Innsbruck
Innrain 52c, 6020 Innsbruck

[c] Univ.-Prof. Dr. H. Grothe
Institute of Materials Chemistry,
TU Wien
Getreidemarkt 9/165, 1060 Wien

Supporting information for this article is available on the WWW under https://doi.org/10.1002/cphc.202400274

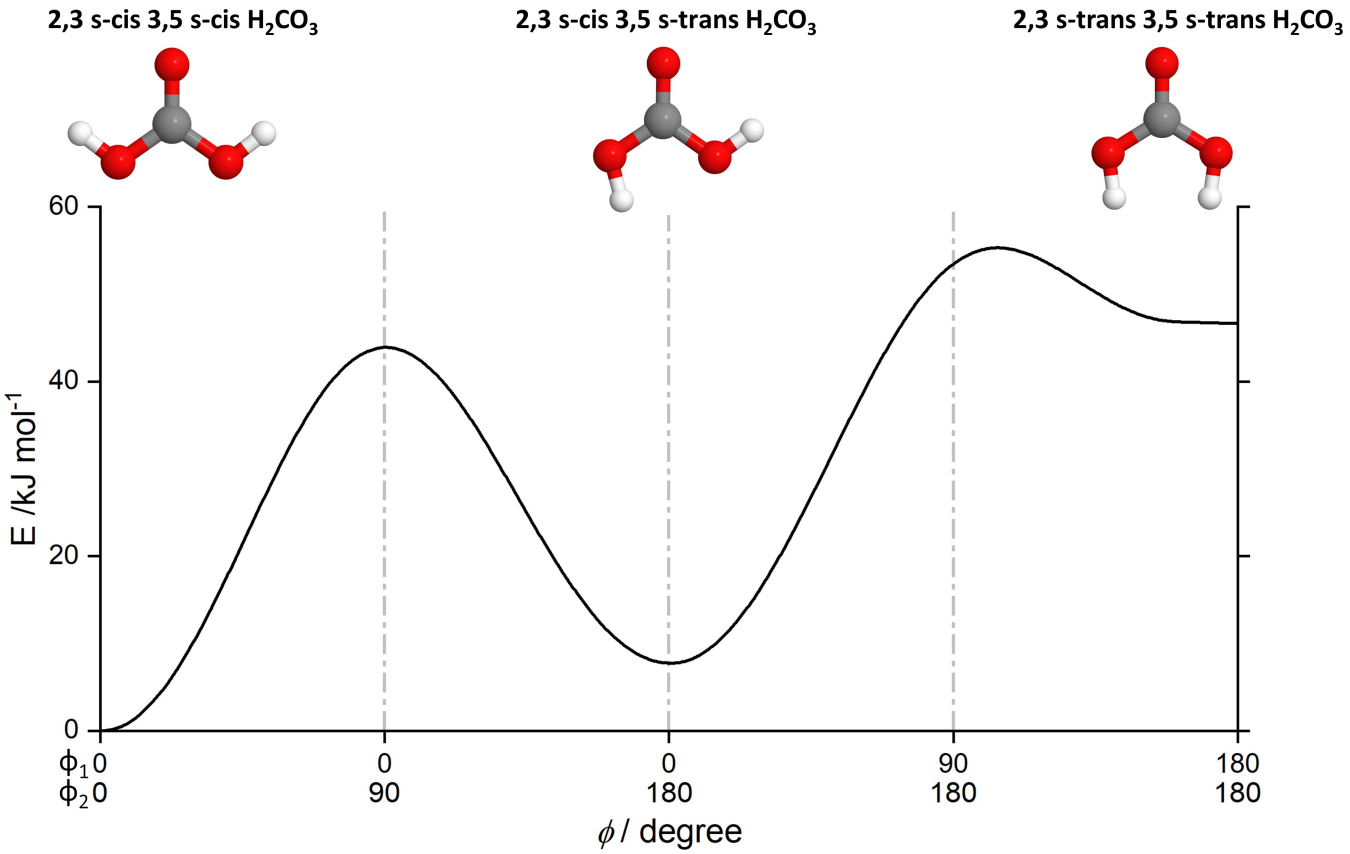

Figure 1. The conformational isomerism of the cc-, ct-, and tt-conformer of carbonic acid can be obtained by changing either OCOH dihedrals. The potential scan was obtained at the CCSD(T)-F12/cc-pVQZ–F12 level of theory with 0.5-degree steps.

laboratory scales under tropospheric conditions, where CA forms in calcite-containing mineral dust and is stable for hours.[4,6]

While most CA synthesis routes lead to the same solid polymorph, the routes established by Hage, Hallbrucker, and Mayer and by Mori et al. suggested three distinct species:[1,2,32] α, β and γ-H_2CO_3. Depending on the solvent in the cryogenic acid-base reaction, one would either yield α-H_2CO_3 by using methanol[1] or β-H_2CO_3 by using water,[2] the latter being identical to CA from other synthesis routes. It was shown that β-H_2CO_3 converts into α-H_2CO_3 upon recrystallization in methanolic solutions, but not *vice versa*.[2]

The study of the phase transition from amorphous to crystalline CA suggested two distinct amorphous forms. It led to the assumption that the then supposed polymorphism of α-H_2CO_3 and β-H_2CO_3 results from polyamorphism.[35] From studying the vibrational frequencies, a cyclic dimer was suggested as the primary building block for β-H_2CO_3.[35] Raman and IR spectra suggested that the rule of mutual exclusion only holds for β-H_2CO_3, assuming an inversion center for the building blocks of β-H_2CO_3 but not for α-H_2CO_3. Consequently, a centrosymmetric dimer was suggested as the building block for β-H_2CO_3 crystals.[36]

The studies on the solid CA culminated in matrix isolation infrared (MI–IR) spectroscopy.[3,6] Matrix isolation allows observation of vibrations of non-rotating single molecules.[37] It turned out that α-H_2CO_3 *is not a polymorph* of CA but carbonic acid monomethyl ester (CAME). The methyl group stems from the methanol solvent in the cryogenic acid-base reaction.[38] Subsequent studies reached the same conclusion[8] and investigated the influence of different solvent materials in different preparation steps.[7]

Early harmonic frequency calculations of CA from 1995 were difficult to verify through the available IR data of solid CA.[25] The access to MI–IR data allowed for the first rigorous assignments from harmonic frequency calculations.[3,6–8] However, harmonic frequency calculations showed significant discrepancies in the experiment. Combination bands and overtones could only be suggested tentatively. This resulted in misassignments, e.g., bands being incorrectly assigned as matrix-induced splitting. Some experimentally observed bands were not assigned at all. Anharmonic frequency calculations can improve the accuracy, as reported in the past,[10,39–42] primarily using vibrational perturbation theory (VPT).

In 2006, Tossell et al.[39] calculated ct-CA and higher dimers using VPT at the B3LYP/CBSB7 level of theory in an aqueous solution using a polarizable continuum solvent model. They concluded that dimers and higher oligomers must be considered, as monomers alone could not explain the solid phase IR spectrum.

In 2011, Reddy et al. suggested linear chains of CA as subunits for CA crystals.[43] In 2012, Reddy et al. redid the

calculations of Tossell et al. and extended their approach to linear tetramers and octamers. They calculated ct-CA, cc-CA, and CA dimers using second-order VPT at MP2 and B3LYP/ 6–311G(2d,d,dp) level of theory. For tetramers, they were limited to the B3LYP level of theory. Based on harmonic-to-anharmonic shifts of the tetramers, they approximated the anharmonic frequencies of the octamers. They conclude that their calculated octamer spectra show a high agreement in the low-frequency areas to the experimental spectra of Loerting and co-workers.

In 2012, Huber et al. recalculated the cc-CA, ct-CA, and CA dimers using second-order VPT at the wB97XD/ aug-cc-pVQZ level of theory for all modes except the OH stretching vibrations.[41] They used a discrete variable representation approach for the highly anharmonic stretching vibrations. Huber et al. demonstrated a good agreement to experiment for cc-CA but only to rough estimates for ct-CA and CA dimers.

In 2024, Fortenberry et al. calculated the rovibrational frequencies of ct-CA and cc-CA using second-order VPT at the CCSD(T)-F12B/cc-pCVTZ–F12 level of theory.[10] They used the SPECTRO program[44] to calculate Fermi resonance polyads, giving them insight into resonance phenomena, where excitation of 2 individual vibrational states is allowed. Furthermore, they generated Cascade emission spectra to compare to interstellar IR data directly.

Using a completely different approach, in 2017, Sagiv et al. solved the time-dependent Schrödinger equation for the OH and CO stretching vibrations.[42] They utilized the *ab initio* classic separable potential (CSP) approach.[45] Gerber et al.[46] showed that for short time scales and systems with moderate quantum effects, the results of CSP agree well with the time-dependent self-consistent field (TDSCF) approach. CSP approximates the multidimensional integrals to TDSCF as averaged values of a set of classical trajectories.[45] The individual single-mode potentials are obtained from classical molecular dynamics trajectories. Mode-coupling is inherently accounted for, as the temporal evolution of the potential allows for energy contributions between the modes. Consequently, the CSP calculations by Sagiv et al. on the CA were the first that accounted for anharmonicity *and* mode-coupling, similar to our calculations mentioned below.

In contrast to these previous studies, we here compute anharmonic spectra for a direct reassignment of the crude MI–IR experimental data. Our computational approach is based on high-level N-mode expansions of the PES with subsequent vibrational self-consistent field and configuration interaction (VSCF/VCI) calculations.[47–49] We demonstrate a significantly improved assignment by comparing the calculations to the MI–IR spectra that were obtained by Bernard et al.[38]

Results and Discussion

Assignment Strategy

Based on VSCF/VCI calculations for ct-H_2CO_3 and cc-H_2CO_3 and their deuterated analogs, we revisit the MI–IR experiments by Bernard et al.[38] and (re)assign several bands. Hereby, we propose a consistent vibrational notation. Usually, the functional group with the largest displacement in a normal mode vector dictates the label of the respective normal mode. While this is appropriate for small molecules, it usually fails for larger molecules with delocalized vibrations. In the case of CA, some vibrations are not well described by this simple notation, as seen from the different notations in literature.[4,8] We here rely on a normal mode decomposition scheme[50–53] using the NOMODECO toolkit[54] to quantify contributions of internal coordinates and provide a more reasonable notation of the vibrational motion. Our assignment strategy is based on the following concepts.

- **Absolute band position**: We compare the experimental and calculated absolute band position. A low discrepancy is usually a good sign for a correct assignment. However, a simple comparison of the absolute band position can be misleading, as there are deviations $>1\,\%$ for individual bands. These deviations are due to non-systematic matrix shifts that occur in the experiment and an error in the anharmonic energy eigenvalue, which is caused by the restriction of the VCI space[55] and the restriction of the multimode expansion of the potential energy surface.[56]
- **Relative band distances**: We calculate the relative band distances, abbreviated as $\Delta\nu^{B2B}$, between two bands in a spectral window, both in the experiment and the calculated spectrum. This band-to-band distance is expected to be less influenced by matrix effects, as in most cases, both bands are prone to similar matrix shifts. A low discrepancy of relative band distances indicates a correct assignment of both bands. Still, as matrix shifts are not systematic, the relative band distances alone can be misleading, too.
- **Intensity/band area ratios**: We calculate the intensity ratio of two bands from the calculated spectra. For the experiment, we calculate the band area ratios. Both ratios are expected to be comparable as they primarily depend on the change in dipole moment. If the ratios of the two bands are similar in experiment and calculation, the assignment can be considered correct. For carbonic acid, the ν_s C=O stretch is always the most intense transition. Hence we abbreviate the intensity/band area ratios as $Q^{\nu\ C=O}$.
- **Normal mode decomposition**: We calculate the normal mode decomposition of the ct- and cc-H_2CO_3 using the NOMODECO toolkit.[54] We observe that vibrations showing similar contributions in the normal mode decomposition also show a similar spectral pattern in the experimental spectrum.

Let us briefly illustrate the assignment strategy on the example of ν_s C=O (ν_2 in the cc-H_2CO_3, ν_3 in the ct-H_2CO_3). The respective spectral region ranges from 1875–1730 cm^{-1}, denoted as the C=O stretching region (cf. Figure 2). The normal mode decomposition (cf. Table 1) confirms this notation, as the

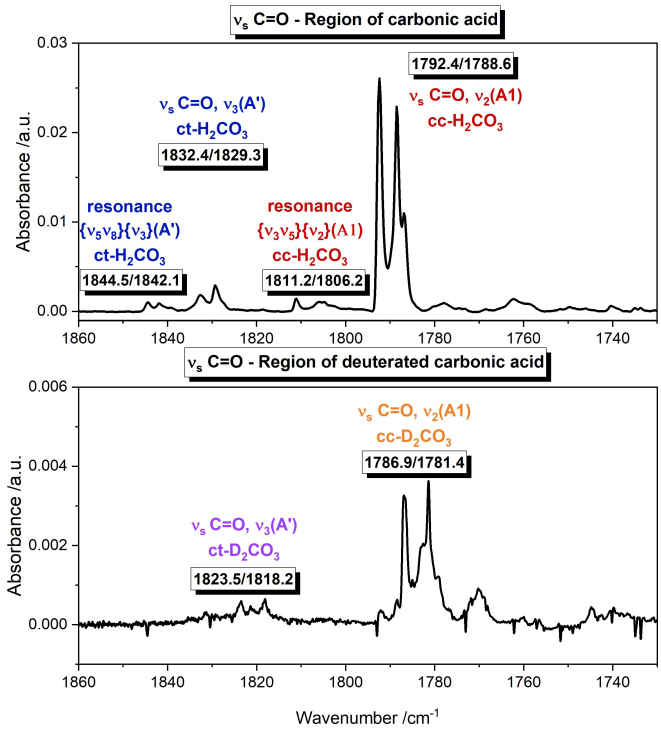

Figure 2. Matrix-isolation IR Spectrum of the C=O stretching region for H_2CO_3 (top) and D_2CO_3 (bottom) in argon.

change in C=O bond length describes over 75% of the normal mode. In the experimental Ar MI–IR data for the protiated species (cf. Figure 2, top), we assign the double-peak (matrix splitting) at 1792.4/1788.6 cm^{-1} as cc-ν_2, or cc-ν_s C=O. Since it is the most intense of the cc-H_2CO_3 vibrations, we take it as a reference to calculate all peak area ratios of the cc-H_2CO_3 bands. The normal mode decomposition of cc-ν_2 and ct-ν_3 is similar (cf. Table 1), hence, we expect a similar peak pattern for these vibrations in the experimental spectrum.

With the VCI calculation resulting in a blue-shifted ct-ν_3 compared to the corresponding cc-ν_2, three double-peaks are candidates to meet the criteria: 1844.5/1842.1, 1832.4/1829.3 and 1811.2/1806.2 cm^{-1}. First and foremost, we attribute the double-peaks to matrix splitting. Considering the band-to-band distance to cc-ν_s C=O, only the second double-peak formation shows a good agreement with the VCI calculated relative band position ($\Delta\nu_{VCI}^{B_2B} = 41\ cm^{-1}$ vs. $\Delta\nu_{exp.}^{B_2B} = 40\ cm^{-1}$). Therefore, the double-peak with the second highest intensity at 1832.4/1829.3 cm^{-1} is assigned as ct-ν_3, or ct-ν_s C=O. The similarity of the peak patterns corroborates the assignment. As it is the most intense vibration in the ct-H_2CO_3 conformer, the peak area ratios of the other bands assigned to the ct-H_2CO_3 conformer refer to this peak.

VCI calculations suggest resonances in the C=O stretching region (cf. Figure 3). For cc-H_2CO_3, the VCI calculated resonance occurs at 1804.9 and 1818.9 cm^{-1} ($\mathcal{Q}_{VCI}^{\nu C=O} = 1:3$). In the experiment, we observe a peak pattern at 1811.2/1806.2 cm^{-1}, which we attribute to matrix-induced splitting, as its band-to-band distance of 5 cm^{-1} agrees to the similar matrix splitting of the cc-ν_2 fundamental in this region. According to the resonance analysis (cf. Figure 3), it is not possible to assign the peak unambiguously, as it has contributions from the $\{\nu_2\}$ and $\{\nu_5\nu_3\}$ configuration. This is an expected consequence of the anharmonic VCI correction, where a better description of the vibrational state is obtained while losing the unambiguity of state assignment. Hence, the most accurate assignment includes both contributing configurations. For ct-H_2CO_3 conformer, the assignment is analogous. The VCI calculated $\{\nu_3\}\{\nu_8\nu_5\}$ resonance occurs at 1845.5 and 1859.5 cm^{-1} ($\mathcal{Q}_{VCI}^{\nu C=O} = 1:3$) and can be assigned to 1832.4 and 1844.5 cm^{-1} in the experiment.

As the C=O stretching vibration example shows, the VCI analysis is a powerful tool for vibrational assignment. We can confidently assign fundamentals of the protiated species as well as the deuterated species. Furthermore, the VCI state analysis also allows us to consider resonating combinations and overtones in the assignment. Which we could otherwise only have assumed since these are not formally allowed in the harmonic approximation. It has already been shown in previous works that the VCI approach can correctly reproduce the Fermi resonance of CO_2 in very good agreement with experimental data.[37,57] Integrating resonances into the assignment of CA allows for the assignment of various bands that could not be previously assigned or were attributed to other effects.

Table 1. Normal mode decomposition of ν_s C=O for the cc-H_2CO_3, ct-H_2CO_3 conformers and their deuterated analogues.

Conformer	Assignment[1]	Frequency[2]	Internal coordinate contributions[3]
cc-H_2CO_3	ν_2	1843	72.68% C=O bond 14.82% C–O bond (7.41% each)
ct-H_2CO_3	ν_3	1894	76.54% C=O bond 12.39% C–O bond (6.43% trans-CO, 5.96% cis-CO)
cc-D_2CO_3	ν_2	1830	73.06% C=O bond 15.02% C–O bond (7.51% each)
ct-D_2CO_3	ν_3	1879	71.20% C=O bond 11.53% C–O bond (5.98% trans-CO, 5.55% cis-CO)

[1] Assignment using the spectroscopic notation.[2] Calculated harmonic frequency in cm^{-1}, using CCSD(T)-F12/cc-pVTZ–F12 level of theory.[3] Internal coordinate contributions calculated via a normal mode decomposition according to Ref. [54].

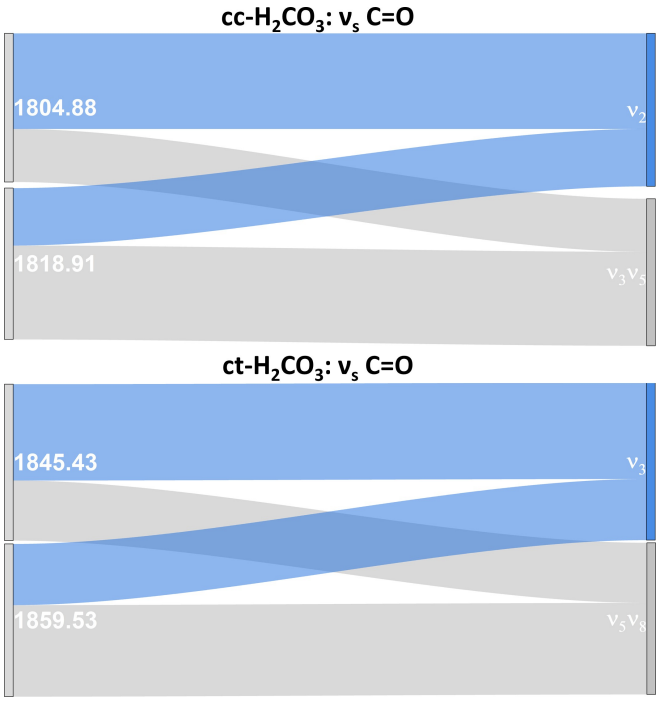

Figure 3. VCI based resonance analysis of ν_s C=O for the cc-H_2CO_3 (top) and ct-H_2CO_3 (bottom) conformation. The Sankey diagrams depict the most significant contributions from the VCI configurations (right) to the VCI-calculated vibrational states (left).

New Assignments

In the following, we explore the reassignments facilitated by VCI analysis (cf. Figure 4, Table 2). The specific assignment of spectral ranges in the SI provides a more detailed overview for the interested reader (cf. SI Figure S2–S17). For the C_{2v} symmetric cc-H_2CO_3, the following vibrations could be newly assigned to an experimental band. We then continue with the vibrations for the C_s symmetric ct-H_2CO_3 that could be newly assigned to an experimental band. Finally, we show the bands that could be newly assigned to an experimental band for the C_{2v} symmetric cc-D_2CO_3.

cc-H_2CO_3 in C_{2v} Symmetry

(1) The ν_s OH vibration, with the spectroscopic label ν_1, has a calculated frequency of $\nu_{VCI}=3671.9\ cm^{-1}$. In line with the deviations between VCI and MI–IR for the other OH stretch vibrations in this region, we would expect to observe the ν_s OH vibration at around 3651–3647 cm^{-1}. However, the ν_s OH vibration has a very low intensity ($\mathcal{Q}_{VCI}^{\nu C=O}=1:52$), so we consider this assignment tentative.

(2) The label $\{\nu_2\}\{\nu_5\nu_3\}$ represents a resonance between the $\{\nu_2\}$ fundamental and a combination $\{\nu_5\nu_3\}$, calculated by VCI at 1818.9 and 1804.9 cm^{-1}. The similar matrix splitting and shape of the bands at 1811.2 and 1792.4 cm^{-1} in the experiment forms the basis for a tenable assignment. The agreement of the calculated and the experimentally observed relative distance between the resonant bands ($\Delta\nu_{VCI}^{B_2B}=14\ cm^{-1}$ vs. $\Delta\nu_{exp.}^{B_2B}=18.8\ cm^{-1}$) further strengthen the assignment.

(3) The $\delta_{ip.\ symm.}$ OH with the spectroscopic label ν_3, has a VCI calculated frequency of $\nu_{VCI}=1250.2\ cm^{-1}$. We assign the experimentally observed band at 1229.2 cm^{-1}. The assignment of this band becomes plausible if we compare the intensity ratios ($\mathcal{Q}_{exp.}^{\nu C=O}=1:17$ vs. $\mathcal{Q}_{VCI}^{\nu C=O}=1:16$). Furthermore, the shoulder at 1227.7 cm^{-1}, which we assign to ct-H_2CO_3 ν_5 (see below), is close in relative proximity both in the experiment and calculation ($\Delta\nu_{exp.}^{B_2B}=1.7\ cm^{-1}$ vs. $\Delta\nu_{VCI}^{B_2B}=5.6\ cm^{-1}$).

(4) The label $\{\nu_4\}\{2\nu_6\}$ represents a resonance between the $\{\nu_4\}$ fundamental and an overtone $\{2\nu_6\}$ within the same symmetry class. The VCI resonance analysis shows for the transition at 1001.4 cm^{-1} a considerable intensity ($\mathcal{Q}_{VCI}^{\nu C=O}=1:22$) and for the transition at 951.7 cm^{-1} a very low intensity ($\mathcal{Q}_{VCI}^{\nu C=O}=1:342$). In the experiment we can assign a band at 1012.2 ($\mathcal{Q}_{exp.}^{\nu C=O}=1:90$). The second feature of this resonance is not observed in the experiment due to its low intensity.

(5) The $\delta_{ip.\ C=O}$ with the spectroscopic label ν_{10}, has a VCI calculated frequency of $\nu_{VCI}=600.3\ cm^{-1}$. We assign the experimentally observed band at 600.8 cm^{-1} due to its very low $\Delta\nu$ of 0.5 cm^{-1} and its very good agreement between calculated and experimentally observed intensity ratio ($\mathcal{Q}_{VCI}^{\nu C=O}=1:8$ vs. $\mathcal{Q}_{exp.}^{\nu C=O}=1:8$).

ct-H_2CO_3 in C_s Symmetry

(1) The two ν OH vibrations, with their respective spectroscopic labels ν_1 and ν_2, have calculated frequencies of $\nu_{VCI}=3634.8\ cm^{-1}$ & $3631.2\ cm^{-1}$. In the experiment, two bands are observed ($\nu_{exp.}=3616.4\ cm^{-1}$ & $3614.5\ cm^{-1}$) that show similar shifts to the OH vibrations of the cc-H_2CO_3 and their relative band distance is in good agreement with the band distance predicted by VCI ($\Delta\nu_{VCI}^{B_2B}=3.6\ cm^{-1}$ vs. $\Delta\nu_{exp.}^{B_2B}=1.9\ cm^{-1}$).

(2) The δ_{ip} OH vibration, with the spectroscopic label ν_5, has a calculated frequency of 1244.6 cm^{-1}. We assign this band to the experimentally observed band at 1227.7 cm^{-1}, in close proximity to the band that we assigned as cc-H_2CO_3 ν_3. Similar to the cc-H_2CO_3 ν_3, the intensity ratios agree well ($\mathcal{Q}_{VCI}^{\nu C=O}=1:3$ vs. $\mathcal{Q}_{exp.}^{\nu C=O}=1:6$).

(3) The δ_{ip} OH vibration with the spectroscopic label ν_6 is in resonance with the first overtone of the ν_{11} according to our VCI analysis. This $\{\nu_6\}\{2\nu_{11}\}$ resonance is calculated at 1179.0 and 1131.9 cm^{-1}. The first feature of the resonance can be assigned to the experimentally observed band at 1181.4 cm^{-1}. The second feature is most likely the band at 1134.7 cm^{-1}, which occurs as a shoulder of the very intense cc-H_2CO_3 ν_9, shifted by 2.5 cm^{-1} in the VCI, resp. by 2.8 cm^{-1} in the experiment. With this assignment, we obtain a good agreement for the band-to-band distance between the two features of the resonance ($\Delta\nu_{exp.}^{B_2B}=46.7\ cm^{-1}$ vs. $\Delta\nu_{VCI}^{B_2B}=47.1\ cm^{-1}$). As the shoulder at 1134.7 cm^{-1} is stronly over-

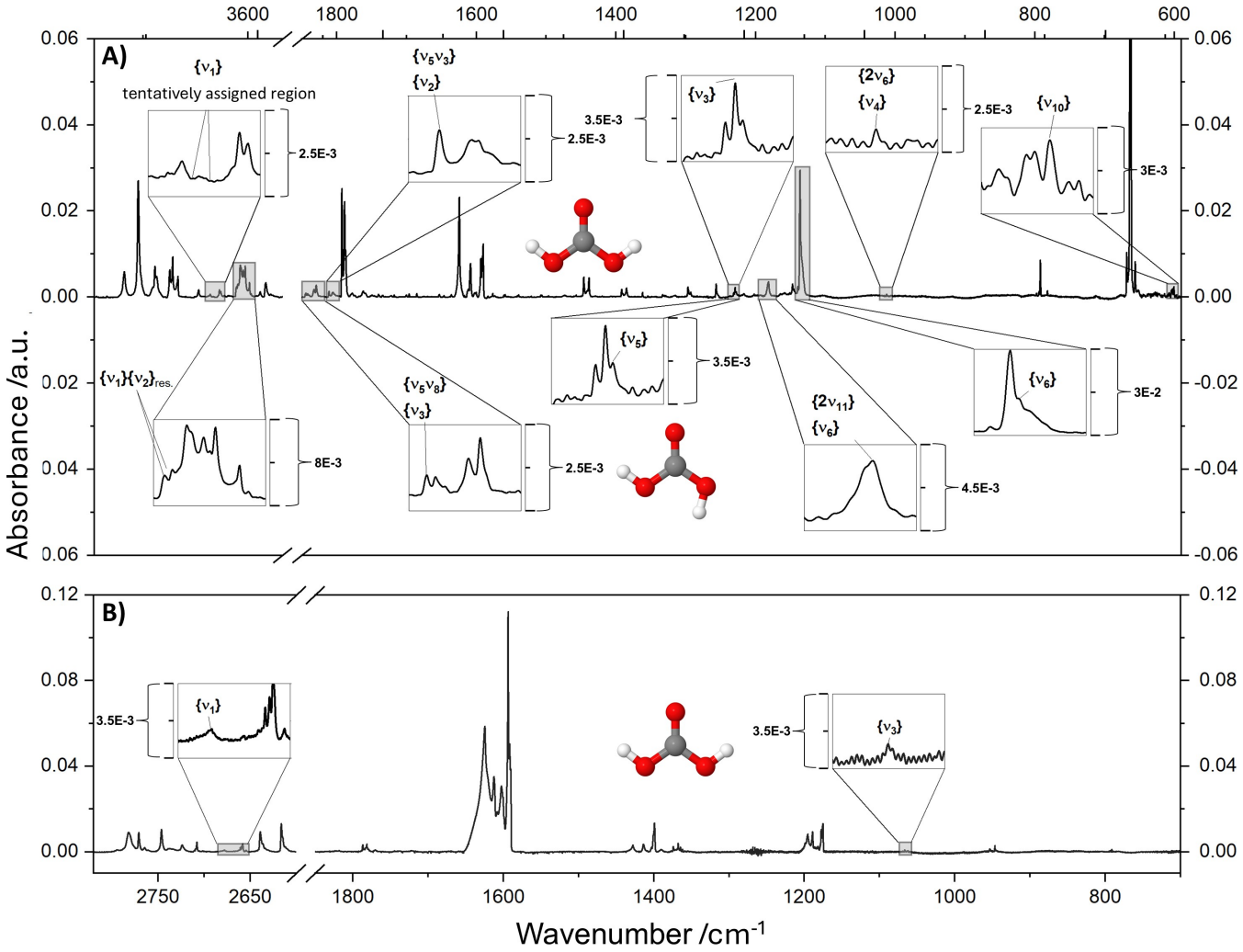

Figure 4. The vibrational matrix-isolation spectrum of H_2CO_3 and D_2CO_3 in argon with newly assigned vibrations as separate windows with the intensities shown as increments for the three species. A.) cc-H_2CO_3 and ct-H_2CO_3 and B.) cc-D_2CO_3. Further spectral regions are shown in the SI (cf. Figures S2-S17).

lapped by the intense cc-H_2CO_3 ν_9, we cannot make a statement about the experimental intensity ratio $\mathcal{Q}_{Int}^{\nu C=O}$.

cc-D_2CO_3 in C_{2v} Symmetry

(1) The ν_s OH vibration, with the spectroscopic label ν_1, has a calculated frequency of 2674.8 cm^{-1}. The calculation agrees well with the experiment ($\nu_{exp.}$ 2677.9 cm^{-1}), and the deviation is in line with other assignments in this region. We observe an overlap with the $1_{11} \leftarrow 0_{00}$ rovibrational transition of water[58] which explains the broad feature that is experimentally observed.

(2) The $\delta_{ip.\,s}$ OH vibration, with the spectroscopic label ν_3, has a calculated frequency of 1061.5 cm^{-1}. The calculations agree well with the experiment, and within $\pm$50 cm^{-1}, no other feature appears in the experiment.

Structural Parameters

Figure 5 summarizes the rotational constants and structural parameters of cc-H_2CO_3 and ct-H_2CO_3. In Table 3, we compare our calculated structural parameters ($\mathbf{r_e}$, $\mathbf{r_a}$, $\mathbf{r_g}$) with the experimental microwave spectroscopy data ($\mathbf{r_0}$) from Mori et al.[32,59] The equilibrium structural parameters ($\mathbf{r_e}$) are obtained from geometry optimizations within the Born-Oppenheimer approximation. The vibrationally averaged structural parameters are from atomic positions averaged over the VCI ground state wavefunction ($\mathbf{r_a}$) or from internuclear distances obtained from an expectation value of the bond lengths expanded in normal coordinates ($\mathbf{r_g}$).[37,60–62]

The comparison in Table 3 must be appreciated carefully. First, the $\mathbf{r_e}$ parameters neglect the nuclear motion and, thus, should poorly agree with parameters from spectroscopic experiments.[62] However, $\mathbf{r_g}$ and $\mathbf{r_a}$ are not necessarily superior to $\mathbf{r_e}$ compared to microwave experiments.[63] In their microwave data, Mori et al. fixed the O–H bond length to the calculated $\mathbf{r_e}$ parameter while fitting the other parameters.[32,59]

Table 2. Experimental mid-IR and calculated vibrational frequencies of cc-H_2CO_3, ct-H_2CO_3, cc-D_2CO_3 and ct-D_2CO_3.

Frequency/cm^{-1} ($\mathcal{Q}_{Int}^{\nu C=O}$)[1]					Assignment[2]		
Ar MI–IR experiment[3]		VCI calculation[4]		$\Delta\nu$	Chemist	Spectroscopic	Γ^{irred}
cc-H_2CO_3							
		3671.9	(1 : 52)		$\nu_{symm.}$ OH	$\{\nu_1\}$	A1
3610.9	(1 : 3)	3637.3	(1 : 3)	26.4 (0.7 %)	$\nu_{anti.}$ OH	$\{\nu_7\}$	B1
1811.2	(1 : 15)	1818.9	(1 : 3)	7.7 (0.4 %)	$\nu_{symm.}$ C=O	$\{\nu_2\}\{\nu_5\nu_3\}$	A1
1792.4	(1 : 1)	1804.9	(1 : 1)	12.5 (0.7 %)			
1445.9	(1 : 5)	1445.1	(1 : 3)	0.8 (0.1 %)	$\nu_{anti.}$ C–O	$\{\nu_8\}$	B1
1229.2	(1 : 17)	1250.2	(1 : 16)	21.0 (1.7 %)	$\delta_{ip.\ symm.}$ OH	$\{\nu_3\}$	A1
1136.1	(1 : 1.4)	1138.5	(1 : 1.2)	2.4 (0.2 %)	$\delta_{ip.\ anti.}$ OH	$\{\nu_9\}$	B1
1012.2	(1 : 90)	1001.4	(1 : 22)	10.8 (1.1 %)	$\nu_{symm.}$ C–O	$\{\nu_4\}\{2\nu_6\}$	A1
		951.3	(1 : 342)				
791.8	(1 : 9)	790.5	(1 : 8)	1.3 (0.2 %)	$\delta_{oop.}$ OCO	$\{\nu_{11}\}$	B2
600.8	(1 : 10)	600.3	(1 : 8)	0.5 (0.1 %)	$\delta_{ip.}$ C=O	$\{\nu_{10}\}$	B1
		546.2	(1 : 2)		$\delta_{oop.\ symm.}$ OH	$\{\nu_{12}\}$	B2
		541.7	(1 : 58)		$\delta_{ip.}$ C–O	$\{\nu_5\}$	A1
		490.4	0		$\delta_{oop.\ anti.}$ OH	$\{\nu_6\}$	A2
ct-H_2CO_3							
3616.4	(1 : 8)	3634.8	(1 : 4)	18.4 (0.5 %)	ν OH	$\{\nu_1\}$	A′
3614.5	(1 : 15)	3631.2	(1 : 10)	17.7 (0.5 %)	ν OH	$\{\nu_2\}$	A′
1844.5	(1 : 2)	1859.5	(1 : 3)	15.0 (0.8 %)	ν C=O	$\{\nu_3\}\{\nu_8\nu_5\}$	A′
1832.4	(1 : 1)	1845.5	(1 : 1)	13.1 (0.7 %)			
1391.7	(1 : 1.2)	1393.6	(1 : 2)	1.9 (0.1 %)	ν C–O	$\{\nu_4\}$	A′
1227.7	(1 : 6)	1244.6	(1 : 3)	16.8 (1.4 %)	$\delta_{ip.}$ OH	$\{\nu_5\}$	A′
1181.4	(1 : 1.3)	1179.0	(1 : 7)	2.5 (0.2 %)	$\delta_{ip.}$ OH	$\{\nu_6\}\{2\nu_{11}\}$	A′
1134.7	–	1131.9	(1 : 3)	2.8 (0.2 %)			
		951.7	(1 : 11)		ν C–O	$\{\nu_7\}$	A′
781.9	(1 : 6)	781.0	(1 : 7)	0.9 (0.1 %)	$\delta_{oop.}$ OCO	$\{\nu_{10}\}$	A″
		605.7	(1 : 30)		$\delta_{ip.}$ C=O	$\{\nu_8\}$	A′
		562.9	(1 : 25)		$\delta_{oop.}$ OH	$\{\nu_{11}\}$	A″
		542.5	(1 : 14)		$\delta_{ip.}$ C–O	$\{\nu_9\}$	A′
		504.2	(1 : 2)		$\delta_{oop.}$ OH	$\{\nu_{12}\}$	A″
cc-D_2CO_3							
2677.9		2674.8		3.7 (0.1 %)	$\nu_{symm.}$ OH	$\{\nu_1\}$	A1
2658.3		2655.0		3.3 (0.1 %)	$\nu_{anti.}$ OH	$\{\nu_7\}$	B1
1781.4		1794.3		12.9 (0.7 %)	$\nu_{symm.}$ C=O	$\{\nu_2\}$	A1
1367.6		1371.5		3.9 (0.3 %)	$\nu_{anti.}$ C–O	$\{\nu_8\}$	B1
1066.5		1061.5		5.0 (0.5 %)	$\delta_{ip.\ symm.}$ OH	$\{\nu_3\}$	A1
946.5		945.4		1.1 (0.1 %)	$\delta_{ip.\ anti.}$ OH	$\{\nu_9\}$	B1
		868.1			$\nu_{symm.}$ C–O	$\{\nu_4\}$	A1
791.3		788.2		3.1 (0.4 %)	$\delta_{oop.}$ OCO	$\{\nu_{11}\}$	B2
		542.2			$\delta_{ip.}$ C=O	$\{\nu_{10}\}$	B1
		494.2			$\delta_{ip.}$ C–O	$\{\nu_5\}$	A1
		433.8			$\delta_{oop.\ symm.}$ OH	$\{\nu_{12}\}$	B2
		415.6			$\delta_{oop.\ anti.}$ OH	$\{\nu_6\}$	A2

[1] The intensity ratios in brackets ($\mathcal{Q}_{Int}^{\nu C=O}$) are given with respect to the strongest absorption, namely ν_s C=O. The discrepancy between experiment and theory $\Delta\nu$ is given as absolute and relative (%) deviation.[2] The *chemist notation* describes the vibration by the largest motion in a normal mode. The *spectroscopic notation* ranks the vibrations according to descending irreducible representation (Γ^{irred}) of the normal mode.[3] Bands are newly assigned based on the original Ar MI–IR data of Bernard.[38] [4] VCI(SDTQ) calculation is based on a n-mode PES expansion with up to 4-mode couplings, computed at CCSD(T)-F12/cc-pVTZ–F12 and CCSD(T)-F12/cc-pVDZ–F12 level of theory, respectively.

Hence, their $\mathbf{r_0}$ parameters are biased and probably cause higher deviation to the $\mathbf{r_a}$ and $\mathbf{r_g}$ parameters than expected. Second, the $\mathbf{r_a}$ and $\mathbf{r_g}$ parameters can have considerable different values.[37,62,64–67] Sometimes, the $\mathbf{r_a}$ parameters of

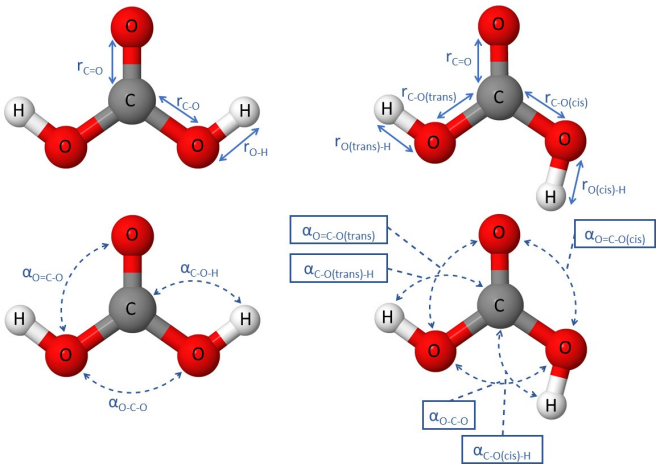

Figure 5. Structural parameters of the cc-H_2CO_3 and ct-H_2CO_3 conformers: bond lengths (top) and bond angles (bottom).

Table 3. Rotational constants (A,B,C) and spectroscopic parameters (bonds r, angles α) of carbonic acid.

	Calc.[1]			Exp.[2]
Parameter	r_e	r_a	r_g	r_0
cc-H_2CO_3				
A/MHz	12029	11950		11997
B/MHz	11363	11280		11308
C/MHz	5484	5795		5814
$r_{C=O}$/Å	1.2026	1.2055	1.2075	1.2024
r_{C-O}/Å	1.3355	1.3426	1.3443	1.3395
r_{O-H}/Å	0.9636	0.9575	0.9820	0.9680*
$\alpha_{O=C-O}$/°	125.67	125.72		125.69
α_{O-C-O}/°	108.65	108.55		
α_{C-O-H}/°	105.93	106.42		105.7
ct-H_2CO_3				
A/MHz	11840	11742		11779
B/MHz	11456	11385		11423
C/MHz	5822	5773		5792
$r_{C=O}$/Å	1.1940	1.1969	1.1989	1.1879
$r_{C-O(t)}$/Å	1.3352	1.3421	1.3438	1.3447
$r_{C-O(c)}$/Å	1.3526	1.3601	1.3617	1.3568
$r_{O(t)-H}$/Å	0.9631	0.9576	0.9823	0.9680*
$r_{O(c)-H}$/Å	0.9637	0.9591	0.9830	0.9680*
$\alpha_{O=C-O(t)}$/°	124.21	124.16		122.94
$\alpha_{O=C-O(c)}$/°	125.19	125.22		126.78
$\alpha_{C-O(t)-H}$/°	108.80	109.30		108.60
$\alpha_{C-O(c)-H}$/°	106.30	106.67		106.10

[1] Equilibrium parameters r_e from geometry optimisation using CCSD(T)-F12/cc-pVTZ–F12 level of theory. Vibrationally averaged parameters r_a and r_g from VCI(SDTQ) calculation, based on n-mode PES expansion with up to 4-mode couplings, computed at CCSD(T)-F12/cc-pVTZ–F12 and CCSD(T)-F12/cc-pVDZ–F12 level of theory, respectively. [2] Experimental parameters r_0 from rotational spectroscopy by Mori et al.,[32,59] where r_{O-H} was fixed (*) to the r_e value.

terminal bonds with a hydrogen atom can be smaller than the corresponding r_e parameter.[65,67] Nevertheless, the VCI calculated vibrationally averaged structural parameters r_a agree well with the experimental data and allow us to distinguish between the cis-sided oxygen and the trans-sided oxygen.

Conclusions

The contemporary interpretation of the H_2CO_3 vibrational spectrum is already quite advanced, owing to matrix-isolation infrared spectroscopy.[3,4,6,8] However, experimental data are still sparse due to the instant decomposition of H_2CO_3, making it difficult to accurately assign all theoretically expected vibrational transitions to experimentally observed bands.

As the complexity of an individual spectrum rises due to, e.g., contaminations, matrix shifts, and resonances (to name but a few), more overlapping bands appear in the spectrum. Empirically shifted harmonic frequencies, even if calculated at a high level of electronic structure theory, are limited in terms of interpretation.[7] At a certain spectral complexity, one has to consider *anharmonicity* and *mode-coupling* to describe certain phenomena that would otherwise be neglected or falsely represented.

Previous anharmonic calculations established a good understanding of the anharmonic shifts of individual carbonic acid vibrations. The most widely used approaches among them are second-order vibrational perturbation approaches (VPT2), which represent an immense improvement compared to calculations within the harmonic approximation.[39–41] Nevertheless, vibrations are still considered as decoupled motions.

The most accurate anharmonic calculations so far by Sagiv et al.[42] showed that the symmetric and antisymmetric OH stretching vibrations have a higher band-to-band distance than in harmonic and the VPT anharmonic approaches.[39–41] However, without a directly accessible reference spectrum, Sagiv et al. could not assign new bands based on their data and only attributed this effect to a higher deviation between experiment and theory. Our VCI calculations led to similar theoretical results, yet by direct comparison with our experimental data, we reevaluated the assignment. Consequently, we reassigned the carbonic acid spectrum of Bernard et al.,[3] which is currently the best experimental recording of a CA spectrum.

We calculated the spectrum of carbonic acid with unprecedented precision, relying on VCI calculations on a 4-mode PES at CCSD(T)-F12/cc-pVTZ–F12 level of theory. These anharmonic corrections and a meticulous assignment strategy allow us to identify several new bands, including resonating overtones and combination bands. While the accuracy of the present calculations is sufficient to interpret the MI–IR data, improvements in the calculations are desirable in future studies. Preliminary results on cc-H_2CO_3 including core-correlation for a 3-mode PES expansion (cf. Table S5) show minor changes that may be essential for predicting the vibrational transitions for gas-phase observations.

We tackle the issue of non-unified vibrational notations, a problem that can lead to comparability issues. Based on normal

mode decomposition,[54] which is numerically reproducible, comparability is guaranteed. Additionally, we show that normal mode decomposition can be utilized during assignment. Whether this is an individual case or a generally applicable rule to aid vibrational assignments must remain the goal of future research.

We want to emphasize that VCI is not a "Black-Box" approach, and the accuracy of the results strongly depends on the accuracy of the PES. Once this is assured, VCI is a powerful tool for vibrational spectroscopy assignments, although the unambiguity of the band assignment is somewhat abandoned. This is particularly evident in the assignment of resonance phenomena in which a fundamental shows the highest contribution to an energy expectation value because, formally, the band is assigned according to the configuration that shows the highest contribution. In the case of these resonances, however, an assignment as a fundamental would not be applicable, as only one energy expectation value can be assigned to a configuration at a time. We circumvent this problem by using the set of configurations as notation and visualizing their respective contributions as Sankey plots (cf. Figures in the SI).

It should be noted here that we did not achieve a complete assignment of the VCI calculated transitions in the experimental spectrum, as some bands of the single molecules were not observed, while others probably arose from either dimers and clusters or from effects not included in the present VSCF/VCI approach (e.g., proton tunneling). Especially fundamentals below 700 cm^{-1} remain unassigned as the mid-IR experiments by Bernard et al. did not cover those low-frequency areas. This region remains to be investigated in future far-IR experiments. However, we were able to newly assign 12 bands of 3 different carbonic acid species (cc-H_2CO_3, ct-H_2CO_3 and cc-D_2CO_3) without deviating significantly from the experiment and without relying on empirical scaling factors.

This study demonstrates the benefits of combining MI–IR spectroscopy and VCI-calculated anharmonic theoretical spectroscopy, further reinforcing the strategy that Dinu et al. have already shown in previous work:[37] Experimental observation hand-in-hand with theoretical predictions work towards the best possible result with less susceptibility to error. Thus, we confidently provide accurate reference data for the vibrational spectrum of carbonic acid. The interstellar existence of carbonic acid is currently being investigated through spectroscopy.[9] Missions like the James Webb Space Telescope can help to show further its existence, but only if sufficiently accurate reference data are available.[10]

Experimental Methods

The matrix-isolation infrared experiments investigated here have been carried out by Jürgen Bernard during his doctoral thesis and partially published in 2012.[38] His PhD supervisor, Thomas Loerting, provided the data. Everything considering the experimental preparation and execution is according to his work.

The preparation of carbonic acid followed a reaction path similar to the one introduced by Hage, Hallbrucker, and Mayer in 1993. A glassy potassium bicarbonate layer was placed on a CsI window at 80 K. Then, a second layer of glassy hydrochloric acid was placed onto the first bicarbonate layer. To start the protonation of the bicarbonate layer, the CsI-window was heated to 180 K. To ensure that the reaction takes place, the whole reaction was observed with a Varian Excalibur IR spectrometer. With a change in the peak pattern in the OH-stretching region, the time-dependent reaction progress could be visibly followed. H_2CO_3 is formed at the start of the reaction and the water is then removed by heating to 210 K. The freshly prepared crystalline carbonic acid was placed into a liquid nitrogen-cooled (77 K) dewar.

Since, at that time, it was not possible to record the matrix-isolation IR spectra at the University of Innsbruck, Jürgen Bernard transported the dewar with the crystalline carbonic acid via train to the laboratory of Hinrich Grothe at the TU Wien. The setup in Vienna was mounted with a UHV Kryostat, allowing for measurements at temperatures around 6 K.[68] A special vacuum load-lock was built to transfer the solid carbonic acid. Inside is a liquid nitrogen-cooled mobile slide with which the sample was transported on the sample holder into the UHV system. The thin layer of hexagonal ice that crystallized during the transfer was removed there. The carbonic acid sample was then sublimated at 210 K and mixed with respective host gas (argon) with a guest-to-host ratio of approximately 1:1000 and deposed on a rotatable gold mirror at a 6 cm distance from the CsI window at 6 K and ultra-high vacuum. The matrix-isolated carbonic acid was then measured with an IR beam.

To ensure that during the transfer and the measurement, no significant contamination or decomposition of the carbonic acid took place, the host material was evaporated at 75 K after the matrix-isolation experiment, and the resulting solid-state IR spectrum was compared to the original solid-state spectrum of the crystalline carbonic acid that was recorded upon preparation.

Computational Methods

All calculations in this work were carried out with the Molpro package 2022.1.[69,70] The geometry optimizations were calculated at the explicitly correlated coupled-cluster theory, considering single, double, and pertubational triple excitations of the cluster operator (CCSD(T)-F12).[71] We used an optimized Dunning basis set (cc-pVTZ–F12)[72] that uses three contracted Gaussian functions per orbital, spanning a total of 22 orbitals (4 outer core orbitals and 18 valence orbitals) and 248 contractions (53 per non-hydrogen atom, and 16 per hydrogen atom). A reference wavefunction is needed to construct the multi-electron wavefunctions from an exponential approach of the cluster operator. Therefore, a restricted Hartree-Fock calculation was performed with a cc-pVTZ–F12 basis set in the first step. Determining the harmonic frequencies and the normal coordinates needed for constructing the potential energy surface (PES) was calculated at the same level of theory, i.e., CCSD(T)-F12/cc-pVTZ–F12.

The construction of the multi-mode potential energy surface (PES) was carried out with a multilevel approach.[73–77] Here again, the same level of theory as before was used for the 1D and 2D coupling terms. And the CCSD(T)-F12/cc-pVDZ level of theory was used for the 3D and 4D coupling terms. The PES is represented along each normal coordinate through 16 equidistant grid points, with the grid size automatically adopted by scaling and shifting.[73] As a starting point for the following vibrational self-consisting field (VSCF) calculation, the PES was transformed from the grid representation into a polynomial representation with polynomials up to the eighth order. For solving the state-specific VSCF calculation, 18 distributed

Gaussian functions were used. The wavefunctions obtained from the VSCF calculations are the starting point for the vibrational configuration interaction calculations. In the calculation, the VCI space is spanned up to five-fold simultaneous excitations, wherein the total count of all excitations must not exceed 15, and the total count of a single excitation must not exceed 5. The VCI calculations not only consider the fundamentals but also combinations and overtones.[49,73,78–81]

Acknowledgements

This research was funded in part by the Austrian Science Fund (FWF) 10.55776/P34518. For open access purposes, the author has applied a CC BY public copyright license to any author accepted manuscript version arising from this submission.

Conflict of Interest

The authors declare no conflict of interest.

Data Availability Statement

The data that support the findings of this study are available in the supplementary material of this article.

Keywords: Ab initio calculations · Carbonic Acid · Matrix isolation · Vibrational configuration interaction · Vibrational spectroscopy

[1] W. Hage, A. Hallbrucker, E. Mayer, *J. Am. Chem. Soc.* **1993**, *115*, 8427.
[2] W. Hage, A. Hallbrucker, E. Mayer, *J. Chem. Soc. Faraday Trans.* **1996**, *92*, 3183.
[3] J. Bernard, R. G. Huber, K. R. Liedl, H. Grothe, T. Loerting, *J. Am. Chem. Soc.* **2013**, *135*, 7732.
[4] J. Bernard, M. Seidl, E. Mayer, T. Loerting, *ChemPhysChem* **2012**, *13*, 3087.
[5] W. Hage, K. R. Liedl, A. Hallbrucker, E. Mayer, *Science* **1998**, *279*, 1332.
[6] J. Bernard, M. Seidl, I. Kohl, K. R. Liedl, E. Mayer, Gálvez, H. Grothe, T. Loerting, *Angew. Chem. Int. Ed.* **2010**, *50*, 1939.
[7] E. Köck, J. Bernard, M. Podewitz, D. F. Dinu, R. G. Huber, K. R. Liedl, H. Grothe, E. Bertel, R. Schlögl, T. Loerting, *Chem. Eur. J.* **2019**, *26*, 285.
[8] H. P. Reisenauer, J. P. Wagner, P. R. Schreiner, *Angew. Chem.* **2014**, *126*, 11960.
[9] M. Sanz-Novo, V. M. Rivilla, I. Jiménez-Serra, J. Martín-Pintado, L. Colzi, S. Zeng, A. Megías, López-Gallifa, A. Martínez-Henares, S. Massalkhi, B. Tercero, P. de Vicente, S. Martín, D. S. Andrés, M. A. Requena-Torres, *J. Astrophys. Astron.* **2023**, *954*, 3.
[10] R. C. Fortenberry, V. J. Esposito, *J. Astrophys. Astron.* **2024**, *961*, 184.
[11] R. King, *Ecyclopedia of Inorganic Chemistry (RA. Scott), Vol 2*, Wiley, Chichester **1994**.
[12] Y. HENDERSON, *J. Am. Med. Assoc.* **1920**, *74*, 783.
[13] D. D. Van Slyke, *J. Biol. Chem.* **1921**, *48*, 153.
[14] A. G. Galinos, A. A. Carotti, *J. Am. Chem. Soc.* **1961**, *83*, 752.
[15] M. Eigen, J. S. Johnson, *Annu. Rev. Phys. Chem.* **1960**, *11*, 307.
[16] B. Jönsson, G. Karlström, H. Wennerström, B. Roos, *Chem. Phys. Lett.* **1976**, *41*, 317.
[17] B. Jönsson, *The Mechanism of Carbonic Anhydrase — A Solvation Problem?, Vol 12*, Springer Netherlands **1979**.
[18] N. M. Tho, T. K. Ha, *J. Am. Chem. Soc.* **1984**, *106*, 599.
[19] R. Khanna, J. Tossell, K. Fox, *Icarus* **1994**, *112*, 541.
[20] N. Jena, P. Mishra, *Theor. Chem. Acc.* **2005**, *114*, 189.
[21] J. Murillo, J. David, A. Restrepo, *Phys. Chem. Chem. Phys.* **2010**, *12*, 10963.
[22] J. Y. Liang, W. N. Lipscomb, *J. Am. Chem. Soc.* **1986**, *108*, 5051.
[23] J. Y. Liang, W. N. Lipscomb, *Biochemistry* **1987**, *26*, 5293.
[24] P. George, C. W. Bock, M. Trachtman, *J. Comput. Chem.* **1982**, *3*, 283.
[25] C. A. Wight, A. I. Boldyrev, *J. Phys. Chem.* **1995**, *99*, 12125.
[26] W. Behrendt, G. Gattow, M. Dräger, *Z. Anorg. Allg. Chem.* **1973**, *397*, 237.
[27] W. Behrendt, G. Gattow, *Z. Anorg. Allg. Chem.* **1973**, *398*, 198.
[28] J. K. Terlouw, C. B. Lebrilla, H. Schwarz, *Angew. Chem. Int. Ed. Engl.* **1987**, *26*, 354.
[29] H. Falcke, S. Eberle, *Water Res.* **1990**, *24*, 685.
[30] M. Moore, R. Khanna, *Spectrochim. Acta Part A* **1991**, *47*, 255.
[31] J. Brucato, M. Palumbo, G. Strazzulla, *Icarus* **1997**, *125*, 135.
[32] T. Mori, K. Suma, Y. Sumiyoshi, Y. Endo, *J. Chem. Phys.* **2009**, *130*, 204308.
[33] T. Loerting, C. Tautermann, R. T. Kroemer, I. Kohl, A. Hallbrucker, E. Mayer, K. R. Liedl, *Angew. Chem. Int. Ed.* **2000**, *39*, 891.
[34] H. A. Al-Hosney, V. H. Grassian, *J. Am. Chem. Soc.* **2004**, *126*, 8068.
[35] I. Kohl, K. Winkel, M. Bauer, K. Liedl, T. Loerting, E. Mayer, *Angew. Chem. Int. Ed.* **2009**, *48*, 2690.
[36] C. Mitterdorfer, J. Bernard, F. Klauser, K. Winkel, I. Kohl, K. R. Liedl, H. Grothe, E. Mayer, T. Loerting, *J. Raman Spectrosc.* **2011**, *43*, 108.
[37] D. F. Dinu, B. Ziegler, M. Podewitz, K. R. Liedl, T. Loerting, H. Grothe, G. Rauhut, *J. Mol. Spectrosc.* **2020**, *367*, 111224.
[38] J. Bernard, available at https://www.loerting.at/publications/bernard14-dissertation.pdf, University of Innsbruck, Ph.D. thesis, Solid and gaseous carbonic acid **2014**.
[39] J. A. Tossell, *Inorg. Chem.* **2006**, *45*, 5961.
[40] S. K. Reddy, C. H. Kulkarni, S. Balasubramanian, *J. Phys. Chem. A* **2012**, *116*, 1638.
[41] S. E. Huber, S. Dalnodar, W. Kausch, S. Kimeswenger, M. Probst, *AIP Adv.* **2012**, *2*, 032180.
[42] L. Sagiv, B. Hirshberg, R. B. Gerber, *Chem. Phys.* **2018**, *514*, 44.
[43] S. K. Reddy, C. H. Kulkarni, S. Balasubramanian, *J. Chem. Phys.* **2011**, *134*, 124511.
[44] J. G. W. G. Handy, SPECTRO: a program for the derivation of spectroscopic constants from provided quartic force fields and cubic dipole fields, in J. M. Bowman, M. A. Ratner (Editors), *Advances in molecular vibrations and collision dynamics*, pages 170–185, JAI Press, Inc., Greenwich, Connecticut **1991**.
[45] B. Hirshberg, L. Sagiv, R. B. Gerber, *J. Chem. Theory Comput.* **2017**, *13*, 982.
[46] P. Jungwirth, R. B. Gerber, *Chem. Rev.* **1999**, *99*, 1583.
[47] J. M. Bowman, K. Christoffel, F. Tobin, *J. Phys. Chem.* **1979**, *83*, 905.
[48] K. M. Christoffel, J. M. Bowman, *Chem. Phys. Lett.* **1982**, *85*, 220.
[49] M. Neff, G. Rauhut, *J. Chem. Phys.* **2009**, *131*, 124129.
[50] Y. Morino, K. Kuchitsu, *J. Chem. Phys.* **1952**, *20*, 1809.
[51] G. Keresztury, G. Jalsovszky, *J. Mol. Struct.* **1971**, *10*, 304.
[52] J. C. Whitmer, *J. Mol. Spectrosc.* **1977**, *68*, 326.
[53] J. A. Boatz, M. S. Gordon, *J. Phys. Chem.* **1989**, *93*, 1819.
[54] K. Oenen, D. F. Dinu, K. R. Liedl, *J. Chem. Phys.* **2024**, *160*, 014104.
[55] T. Mathea, available at https://elib.uni-stuttgart.de/handle/11682/12176, *Universität Stuttgart, Ph. D thesis,* Fortgeschrittene Konzepte zur Identifizierung und effizienten Berechnung von Schwingungszuständen innerhalb des VCI-Verfahrens, **2022**.
[56] D. Oschetzki, available a thttps://elib.uni-stuttgart.de/handle/11682/8998, *Universität Stuttgart,Ph. D thesis,* Entwicklung akkurater und effizienter Schwingungskorrelationsverfahren zur Simulation anharmonischer Schwingungsspektren für größere Moleküle und molekulare Cluster, **2016**.
[57] V. Rodriguez-Garcia, S. Hirata, K. Yagi, K. Hirao, T. Taketsugu, I. Schweigert, M. Tasumi, *J. Chem. Phys.* **2007**, *126*, 124303.
[58] D. F. Dinu, M. Podewitz, H. Grothe, K. R. Liedl, T. Loerting, *J. Phys. Chem. A* **2019**, *123*, 8234.
[59] T. Mori, K. Suma, Y. Sumiyoshi, Y. Endo, *J. Chem. Phys.* **2011**, *134*, 044319.
[60] N. Lucas, *Mol. Phys.* **1972**, *23*, 825.
[61] I. M. Mills, *J. Phys. Chem.* **1976**, *80*, 1187.
[62] G. Czakó, E. Mátyus, A. G. Császár, *J. Phys. Chem. A* **2009**, *113*, 11665.
[63] D. F. Dinu, M. Podewitz, H. Grothe, T. Loerting, K. R. Liedl, *Theor. Chem. Acc.* **2020**, *139*, 174.
[64] M. Tschöpe, B. Schröder, S. Erfort, G. Rauhut, *Front. Chem.* **2021**, *8*, 1.

[65] S. Erfort, M. Tschöpe, G. Rauhut, *J. Chem. Phys.* **2022**, *156*, 124102.
[66] M. Tschöpe, *J. Astrophys. Astron.* **2023**, *949*, 1.
[67] M. Tschöpe, G. Rauhut, *Mon. Not. R. Astron. Soc.* **2023**, *520*, 3345.
[68] O. Gálvez, A. Zoermer, A. Loewenschuss, H. Grothe, *J. Phys. Chem. A* **2006**, *110*, 6472.
[69] H. Werner, P. J. Knowles, G. Knizia, F. R. Manby, M. Schütz, *WIREs Comput. Mol. Sci.* **2011**, *2*, 242.
[70] J. P. Wagner, H. P. Reisenauer, V. Hirvonen, C.-H. Wu, J. L. Tyberg, W. D. Allen, P. R. Schreiner, *Chem. Commun.* **2016**, *52*, 7858.
[71] T. B. Adler, G. Knizia, H.-J. Werner, *J. Chem. Phys.* **2007**, *127*, 221106.
[72] T. H. Dunning, *J. Chem. Phys.* **1989**, *90*, 1007.
[73] G. Rauhut, *J. Chem. Phys.* **2004**, *121*, 9313.
[74] P. Meier, Dissertation, *Universität Stuttgart* **2014**.
[75] B. Ziegler, G. Rauhut, *J. Chem. Phys.* **2016**, *144*, 114114.
[76] B. Ziegler, G. Rauhut, *J. Chem. Phys.* **2018**, *149*, 164110.
[77] B. Ziegler, G. Rauhut, *J. Chem. Theory Comput.* **2019**, *15*, 4187.
[78] G. Rauhut, T. Hrenar, *Chem. Phys.* **2008**, *346*, 160.
[79] T. Hrenar, H.-J. Werner, G. Rauhut, *J. Chem. Phys.* **2007**, *126*, 134108.
[80] T. Mathea, G. Rauhut, *J. Chem. Phys.* **2020**, *152*, 194112.
[81] T. Petrenko, G. Rauhut, *J. Chem. Phys.* **2017**, *146*, 124101.

Manuscript received: March 12, 2024
Revised manuscript received: July 12, 2024
Accepted manuscript online: July 19, 2024
Version of record online: October 25, 2024